Journal of Materials Chemistry A

PAPER

View Article Online
View Journal | View Issue

Cite this: J. Mater. Chem. A, 2017, 5, 6914

Uni-directional liquid spreading control on a bio-inspired surface from the peristome of *Nepenthes alata*†

Huawei Chen, ‡*[a] Liwen Zhang, ‡[a] Yi Zhang,[a] Pengfei Zhang,[a] Deyuan Zhang[a] and Lei Jiang[b]

Received 21st February 2017
Accepted 13th March 2017

DOI: 10.1039/c7ta01609c

rsc.li/materials-a

Uni-directional liquid spreading without energy input has gained much attention due to its potential application in various areas such as microfluidic devices and energy fields. Recently, continuous uni-directional liquid spreading with fast speed was discovered on the peristome of *Nepenthes alata*, which possesses superhydrophilic hierarchical microgrooves and duck-billed microcavities with arc-shaped edges and gradient wedge corners. Inspired by the surface structure of the peristome, a novel bio-inspired uni-directional liquid spreading surface with various arc curvatures and wedge angles was built *via* two-step inclined UV exposure photolithography. The effects of the surface wettability and structural features, *i.e.* the arc-shaped outlines and wedge corners of microcavities, on the anisotropy of liquid spreading were investigated. The underlying mechanisms were made clear by comparing the effects of surface wettability and structural features of microcavities on both liquid spreading ability and liquid pinning ability. Finally, the controlling of anisotropic liquid spreading and thorough uni-directional liquid spreading were realized. This study provides inspiration to design novel uni-directional liquid spreading surfaces without energy input, and can further expand their application in areas such as non-powered delivery systems, microfluidic devices and self-lubrication in mechanical engineering.

1. Introduction

Uni-directional liquid spreading without energy input has attracted worldwide attention in recent years for its diverse potential applications, in areas such as non-powered delivery systems, self-lubrication and microfluidic devices.[1–9] Directional liquid spreading systems are mainly constructed through combining surfaces with gradient or patterned wettability[8,10–14] and structures with gradient Laplace pressures, *e.g.*, a 1D conical spine with a hydrophilic surface,[2,3,15,16] a conical tube with a hydrophilic surface[17] and hydrophilic inclined micropillar arrays.[18] In past years, the control of directional liquid spreading abilities has been explored either through adjusting the surface wettability *via* pH values, temperature and exposure to UV light,[19–22] or through the optimization of structural features such as the apex angle in cactus spines[15,23] and micropillar heights.[18] Besides, the effects of surface wettability and structural features are sometimes interlinked. However, the application of these directional liquid spreading structures is still in progress, due to their slow spreading speeds and short spreading distances.[24,25]

Recently, we have discovered uni-directional liquid spreading on the peristome of *N. alata*, which is mainly as a result of its unique superhydrophilic hierarchical structure and duck-billed microcavities with arc-shaped edges and sharp wedge corners.[26] However, the effects of surface wettability and each structural feature extracted from the peristome on uni-directional liquid spreading abilities are still not clear, which makes it a very necessary topic to be investigated. The mechanism of continuous spreading in the front direction and pinning in the opposite direction also needs to be studied.

Under the inspiration of *N. alata*, one novel bio-inspired uni-directional liquid spreading surface is proposed and fabricated *via* two-step inclined UV exposure photolithography.[27] The impacts of surface wettability and structural features on anisotropic liquid spreading are investigated through comparing the spreading speeds and spreading distances of liquids on uni-directional spreading surfaces that are constructed with varying surface wettability and structural parameters. Finally, the underlying mechanisms of anisotropic liquid spreading are explored. The anisotropy of liquid spreading can be controlled, and the building of thorough uni-directional liquid spreading surfaces is studied.

[a]School of Mechanical Engineering and Automation, Beihang University, Beijing, 100191, China. E-mail: chenhw75@buaa.edu.cn

[b]Laboratory of Bio-inspired Smart Interface Science, Technical Institute of Physics and Chemistry, Chinese Academy of Sciences, Beijing, 100190, China

† Electronic supplementary information (ESI) available: Videos of liquid spreading on surface structures with different arc edge curvatures and microcavity wedge angles β. Video of pinning failure. See DOI: 10.1039/c7ta01609c

‡ These authors contributed equally to this work.

2. Results and discussion

2.1 Control of surface wettability on uni-directional spreading

The intrinsic superhydrophilicity of the peristome of *N. alata* demonstrates that surface wettability is one key factor for the uni-directional spreading of water. To test the effect of surface wettability on uni-directional liquid spreading, surfaces with varying wettability with one typical anisotropic structure were obtained *via* the use of different oxygen plasma treatment times. When the contact angle is about 64°, water shows no spreading. With a surface wettability close to superhydrophilic, the uni-directional water spreading properties become more obvious (Fig. 1a). Generally, the spreading speed and spreading distance increase as the contact angle drops (Fig. S1a†). Thus, a superhydrophilic surface can achieve a perfect uni-directional liquid spreading performance, as shown in Fig. 1b. Even for liquids with high viscosity, *e.g.* silicon oil with viscosities of 50, 100 and 350 $mm^2\ s^{-1}$, uni-directional liquid spreading still can be obtained (Fig. 1c). However, the spreading speed in the front direction decreases with an increase in viscosity. The final spreading distances for the same volume of liquid with different viscosities are similar, indicating that the uni-directional spreading abilities of one bio-inspired surface, especially the spreading distance, mainly depend on surface wettability (Fig. S1b†).

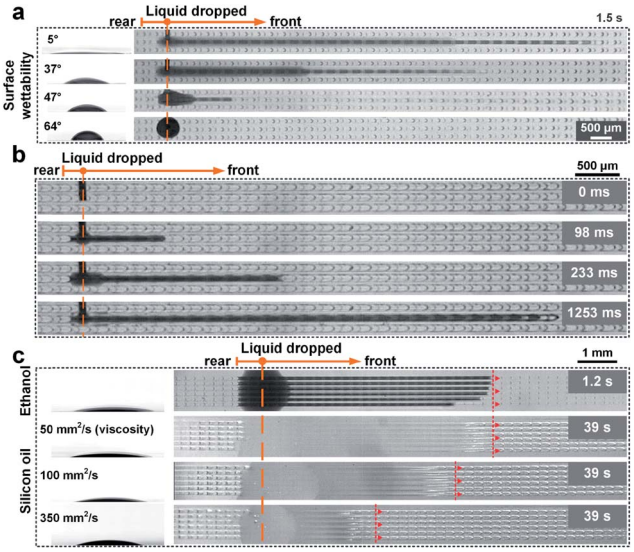

Fig. 1 Effects of surface wettability on uni-directional spreading. (a) ~0.1 μL of water spreading with different surface wettability. Only the wettable surface demonstrates uni-directional spread on this surface structure. The water almost stops spreading after the contact angle reaches about 64°. (b) Uni-directional liquid spreading on a super-hydrophilic bio-inspired surface. (c) Uni-directional spreading with different liquid viscosities, including ethanol and silicon oil with viscosities of 50, 100 and 350 $mm^2\ s^{-1}$. A liquid droplet of ~1 μL is dropped onto six parallel arranged microgrooves. The dashed line denotes the place where the liquid is dropped.

2.2 Impact of two structural features on uni-directional spreading

The bio-inspired surface structure consists of two layers. Isometrical inclined arc stages and pit arrays are linearly aligned as the bottom layer, and straight microgrooves are overlaid on these stages and pits to form the upper layer (Fig. 2a). Here, we define the arc edge convex side as the front direction, and its opposite side as the rear direction. Comparing the section view of A–A in Fig. 2b and the duck-billed microcavities of the *N. alata* peristome surface, two typical structural features should have a great impact on uni-directional liquid spreading, involving the arc edge curvature and the wedge angle β of microcavities. To make clear their effects on anisotropic liquid spreading, a variety of arc edges, including straight (S), circle arc (C) and ellipse arc (E), were prepared with an increase in curvature, and a variable wedge angle β ranging from ~50° to ~110° (Fig. S2†).

2.2.1 Influence of arc edge curvature. A variety of arc edges were fabricated to study the effect of arc edge curvature, including straight (S), a circle arc with a radius of 60 μm (C60), and ellipse arcs with semi-major axis lengths of 110, 150 and 190 μm (E110, E150 and E190), as shown in Fig. 3a. The wedge angle β of the microcavities is set to 50°, with other structural parameters remaining the same (Fig. S3†). About 0.1 μL of ethanol was used and injected into the center of these microgrooves in about 0.1 s (Video S1†). By comparing the liquid spreading state after 1.5 s (Fig. 3b), anisotropic liquid spreading generally becomes more significant with an increase in arc edge curvature. Notably in respect to S and C60, liquid cannot be effectively pinned and spreads a short distance in the rear direction. Because the wedge angle β exists in S as the sole anisotropic structural feature, the liquid spreads slightly further in the front direction than in the rear direction. As for C60, the arc edge is another type of structural anisotropy besides the wedge angle β and leads to a higher anisotropic liquid spreading factor ξ_d ~0.5, which is defined as

$$\xi_d = \frac{|d_f - d_r|}{\max(d_f, d_r)} \quad (1)$$

where d_f and d_r are the spreading distances of the liquid in the front and rear directions respectively at same time interval. Particularly, with regard to E110, E150 and E190, the anisotropic liquid spreading effects become much stronger with an increase in the arc edge curvature, and finally thorough uni-

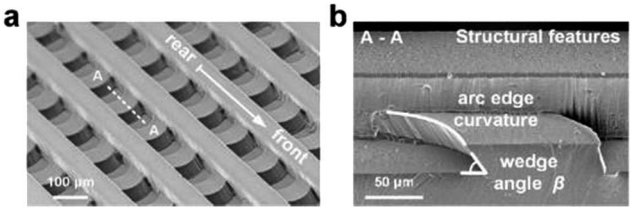

Fig. 2 The structure of uni-directional liquid spreading surface. (a) SEM image of bio-inspired uni-directional liquid spreading surface. (b) Section view A–A of the surface structure. Two main features have been extracted as attributes of the structure, *i.e.* curvature of arc edge and wedge angle of microcavity β.

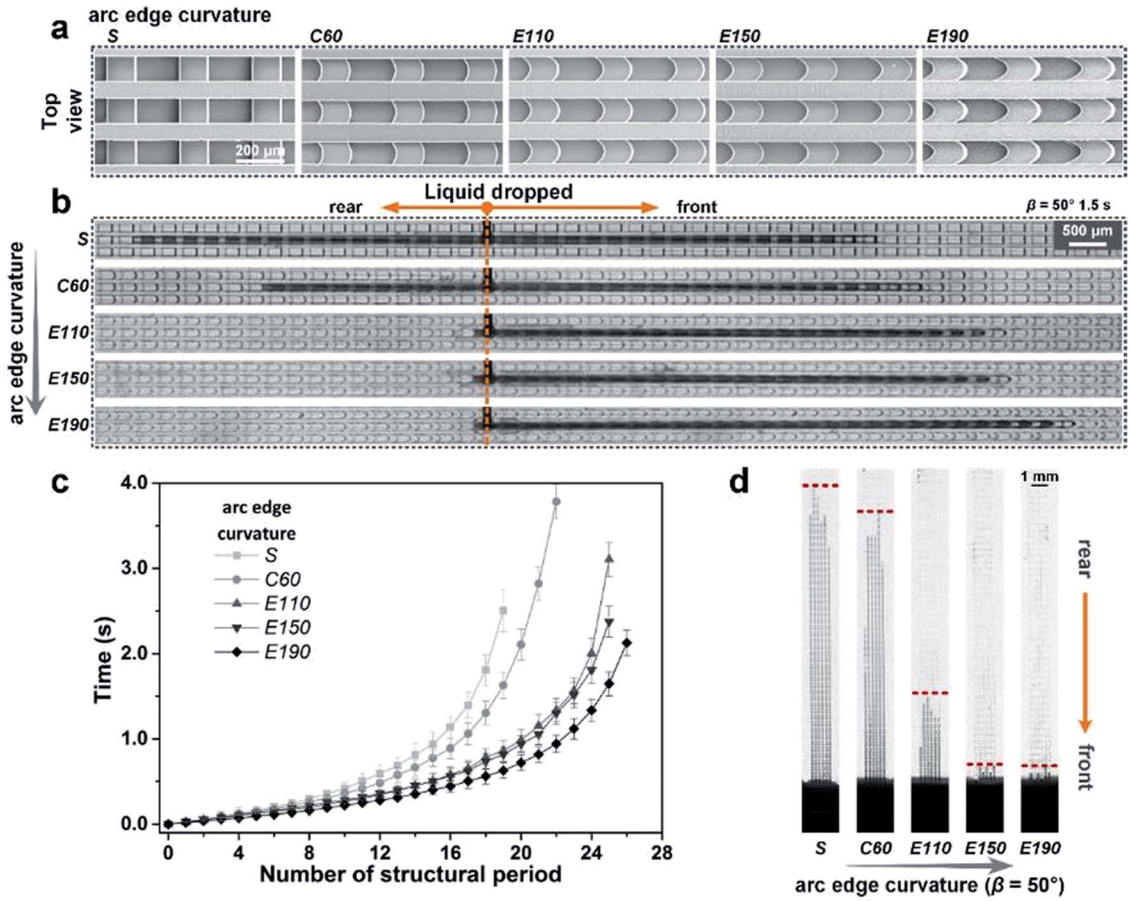

Fig. 3 Effects of different arc edge curvatures on liquid spreading in surface structures. (a) SEM images of surface structures with five types of arc edge curvature include straight (S), circle arc with a radius of 60 μm (C60) and ellipse arc with semi-major axis lengths of 110, 150 and 190 μm (E110, E150 and E190). (b) *In situ* observation of five types of surface structure with a microcavity wedge angle β of 50° at a time of 1.5 s. The dashed line denotes the place liquid was dropped. (c) Time needed for liquid spreading to pass structural periods on five types of surface in the front direction. (d) The pinning ability comparison was conducted by immersing the structures with the front direction vertically down into the liquid. Dashed lines show the height of liquid climbing after 11 s in the reverse direction.

directional liquid spreading appears with ξ_d close to 1 (Fig. S4a†). Apart from the anisotropic spreading ability, the spreading speeds and final spreading distances in the front direction have also been collected (Fig. 3c). In general, the spreading speed in the front direction gradually declines with the increase in spreading distance. Especially, it is obvious that both spreading speed and final spreading distance in the front direction rise with the increase in arc edge curvature. To explore the liquid pinning ability much deeper, these surface structures were vertically immersed into liquid with the front direction of the surface structure downwards. As shown in Fig. 3d, the pinning ability of S and C60 is quite weak since liquid quickly climbs up. As for ellipse arc surface structures, though all of them demonstrate much stronger uni-directional liquid spreading abilities, their pinning abilities are still different. The larger the arc edge curvature is, the stronger the pinning ability appears. Among the ellipse surface structures, E190 shows the strongest pinning ability, with a liquid climbing height lower than E150 and about three times less than E110 (Fig. S4b†).

2.2.2 Influence of wedge angle β. The influence of microcavity wedge angle β was also investigated through a comparison of liquid spreading in four types of surface structures with different wedge angles. Fig. 4a shows scanning electron microscope (SEM, Model JSM-6010LA, JEOL, Ltd.) images of surface structures with a wedge angle β of about 50°, 70°, 90° and 110°. The arc edge curvature of the microcavities is designed as E190, and other structural parameters remain the same (Fig. S3†). After dropping 0.1 μL of ethanol into the center of the microgrooves (Fig. 4b & Video S2†), the surface structure with a wedge angle β of 110° cannot keep the liquid pinned in the rear direction, with the weakest ξ_d, of about 0.5 (Fig. S4c†). However, for the surface structure with a wedge angle β of 50°, uni-directional liquid spreading appears, indicating that the uni-directional liquid spreading gradually becomes stronger with the decline in wedge angle β. Of course, the spreading speed and final spreading distance in the front direction also decrease with the increase in wedge angle β, as shown in Fig. 4c. In the reverse immersing experiments (Fig. 4d), the surface structure with the sharpest wedge angle, $\beta = 50°$, shows the

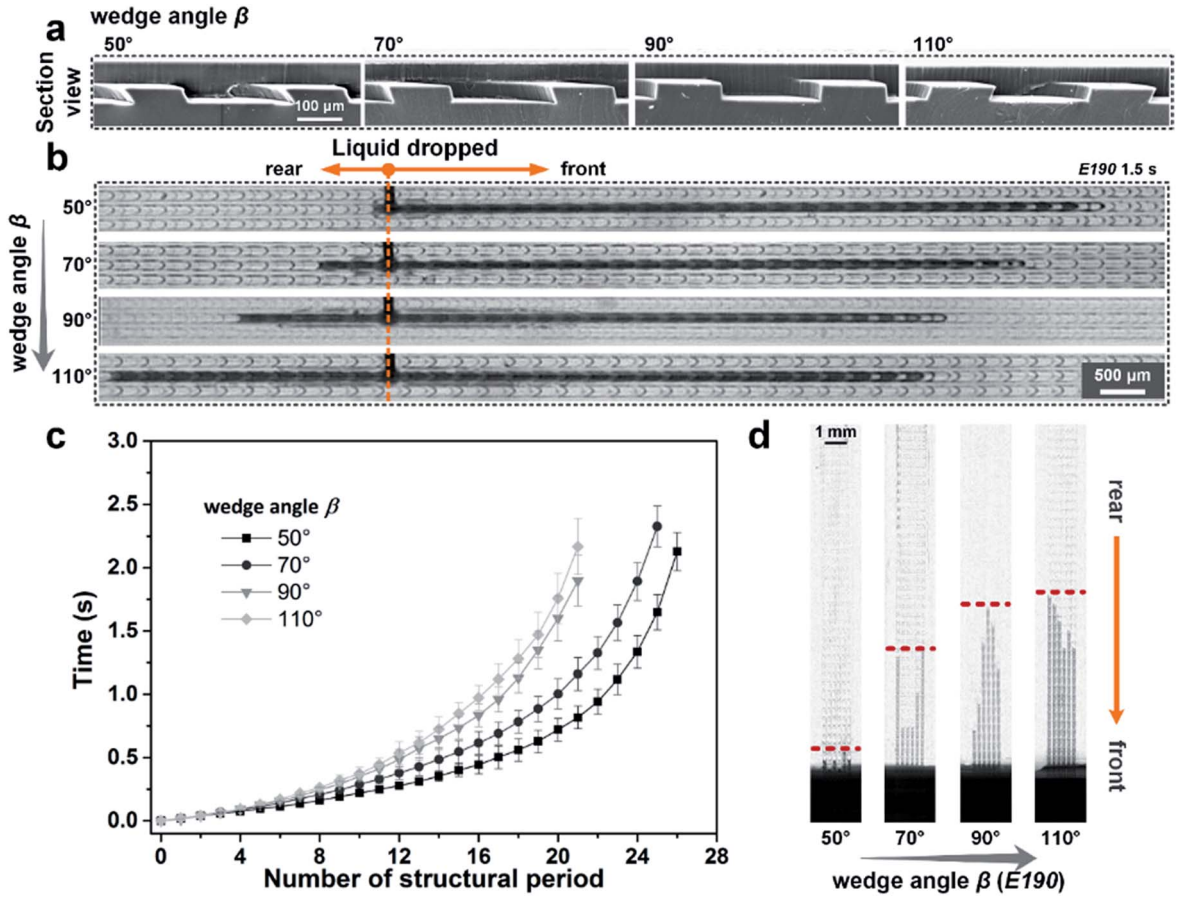

Fig. 4 Effects of different microcavity wedge angles β on liquid spreading in surface structures. (a) SEM images of surface structures with wedge angles β of about 50°, 70°, 90° and 110°. (b) *In situ* observation of four different β surface structures with an arc edge curvature of E190 at a time of 1.5 s. The dashed line denotes the place where the liquid was dropped. (c) Time needed for liquid spreading to pass structural periods on four types of surface in the front direction. (d) The pinning ability comparison was conducted by immersing the structures with the front direction vertically in the liquid. The dashed lines show the height of liquid climbing after 11 s in the reverse direction.

strongest pinning ability with the lowest climbing height, and the climbing height gradually is enhanced as the wedge angle increases (Fig. S4d†).

2.3 The underlying mechanisms of uni-directional liquid spreading control

2.3.1 Microscopic characteristics of the structural features for uni-directional spreading. To reveal the mechanisms underpinning anisotropic liquid spreading, *in situ* microscopic observation of liquid spreading on the surface structures are conducted. The precursor of liquid spreading in different surface structures is compared, as shown in the right side of Fig. 5a. In the case of E190, with a β value of 50°, the liquid spreading precursor in the front direction appears much sharper with a longer length L and a smaller width D. In the rear direction, section views of liquid pinning states at the edge center are obtained using a laser confocal microscope (Model LSM780, Zeiss) as shown on the left side of Fig. 5a. The liquid in E190 with a β value of 50° can be pinned at the edge with a large apparent contact angle and thick liquid film. When pinning failure happened, liquid in the surface structure with a β value of 50° and a small arc edge curvature C60 always breaks through pinning at the intersection of the arc edge and microgroove wall, and then flows into the pits (Fig. 5b, left side & Video S3†). While in E190 with a large wedge angle β of 110°, pinning failure occurs with liquid rushing into the pits through the center of the arc edge (Fig. 5b, right side).

2.3.2 Mechanism for liquid spreading. The cooperative effects of surface wettability and two typical structural features are attributed to liquid spreading in the front direction and pinning in the rear direction, which leads to uni-directional liquid spreading. Liquid spreading on the bio-inspired surface structure generally is fulfilled by the continuous climbing of liquid across each stage and then filling the next pit. In the duration of pit filling, liquid initially spreads along the bottom corner of the pit flank, and then gathers at the apex of the microcavity. Bio-inspired surface structures with different arc edge curvatures and microcavity wedge angles β exhibit distinct liquid spreading characteristics, as shown in the top view of the front direction (Fig. 5a, right side). In the case of E190 with a β value of 50°, its longer L and smaller D denote that it possesses strong spreading and filling abilities. The impact of this on liquid spreading induced by arc edge curvature and microcavity wedge angle β can

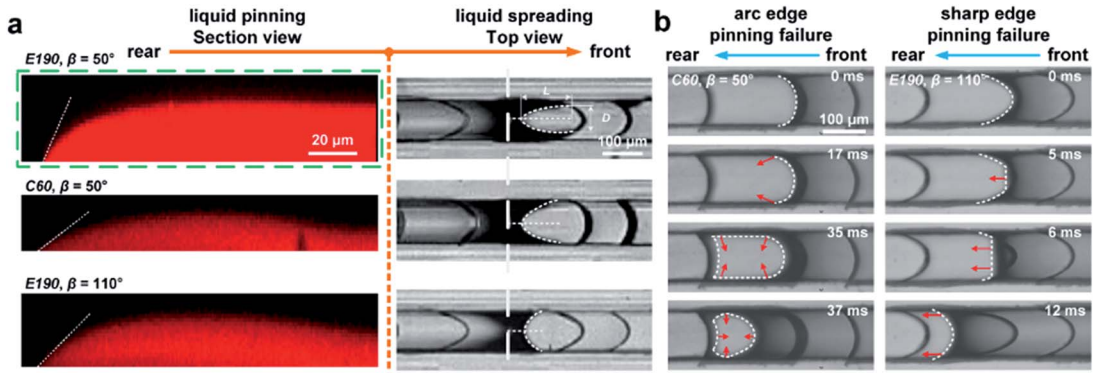

Fig. 5 Microscopic view of liquid spreading and pinning in different surface structures. (a) In the rear direction (left side), section views of the liquid's steady pinning state at the center of the edge have been compared. E190, $\beta = 50°$ has the thickest liquid film and forms the largest apparent contact angle at the arc edge. In the front direction (right side), the precursors of spreading liquid have been captured, and E190, $\beta = 50°$ has the sharpest precursor with the longest length L and the smallest width D. (b) When pinning failure happened, liquid on the surface with a small arc edge curvature (C60, $\beta = 50°$, left side) spreads through the intersection of the arc edge and microgroove wall, while liquid on the surface with a large wedge angle β (E190, $\beta = 110°$, right side) breaks the pinning barrier through the center of the arc edge. Red arrows show the direction of liquid spread.

be regarded as two kinds of capillary rise effects, *i.e.* in taper and in wedge corner (Fig. 6a and b).

The open angle η, formed by the liquid precursor at position l and the apex of the arc edge (Fig. 6a, top), can be viewed as a taper with a cone angle of α_1 (Fig. 6a, bottom). In the taper, the height of stable liquid capillary rising can be defined as

$$h_1(\alpha_1) = \frac{H}{2}\left[1 - \sqrt{1 - \frac{4\gamma}{\rho g H^2} \times \frac{\cos(\theta - \alpha_1/2)}{\tan(\alpha_1/2)}}\right] \quad (2)$$

where γ, θ, ρ, g and H denote the liquid surface tension, the liquid contact angle, the liquid density, the gravitational acceleration and the height of the wedge corner, respectively.[28] It is clear that with the decline of the cone angle α_1, the height of capillary rising h_1 will be enhanced. Since the open angle η is smaller with a larger arc edge curvature, *e.g.*, $\eta_E < \eta_C$ (Fig. 6a, top), the liquid spreading ability for a larger arc edge curvature will be better, which explains the strong liquid spreading performance in E190 (Fig. 3b and c).

In the case of liquid spreading in a wedge microcavity (Fig. 6b, top), the changing of the wedge angle β can be regarded as a wedge corner with various angles α_2 (Fig. 6b, bottom). The height of a stable liquid capillary rising in a wedge corner is

$$h_2(\alpha_2, x) = \frac{2\gamma\cos\theta}{\rho g x \alpha_2} \quad (3)$$

where x denotes the distance from the liquid precursor to the apex of the corner.[26] With a smaller corner angle α_2, a higher h_2 can be achieved. Then, in a bio-inspired surface with a smaller wedge angle β, stronger liquid spreading abilities can be achieved, which is in perfect accordance with the fastest spreading speed and longest spreading distance occurring in the case of the smallest wedge angle β of 50° in Fig. 4b and c. Due to both stable capillary rise heights h_1 and h_2 increasing with a smaller contact angle θ, stronger surface wettability will lead to liquid spreading in the front direction being much easier. This explains why the peristome surface of *N. alata* is superhydrophilic for uni-directional water spreading. Combining the effect of surface wettability and two structural features, liquid spreading ability in the front direction can be controlled.

2.3.3 Mechanism for liquid pinning. Liquid pinning in the rear direction is another crucial factor for uni-directional liquid spreading. The large apparent contact angle and thick liquid film forming at the edge in E190 with a β value of 50° demonstrates that two structural features can jointly enhance the liquid pinning effect in the rear direction (Fig. 5a, left side). The liquid thickness of the pinned liquid in the rear direction gradually decreases along the corner A (CA) that is formed by the microgroove wall and the top of the pit stages (Fig. 6c), which means that the apparent contact angle regularly declines from the apex of the arc edge to the intersection of CA and the rear edge (RE). With the decline in arc edge curvature (from E to C), the apparent contact angle of the pinned liquid at the intersection of CA and RE gradually becomes larger, and arc edge pinning effects become much weaker. The liquid will easily break through pinning at the intersection and then flow into pits, *e.g.*, a liquid pinning failure for the small arc edge curvature C60 with a β value of 50° (Fig. 5b, left side & 6c). With an increase in wedge angle β (from 50° to 110°), pinning at RE can be penetrated because of the lower sharp edge pinning effect.[29] In E190 with a large wedge angle β of 110°, pinning failure occurs with liquid rushing into pits through the center of the arc edge (Fig. 5b, right side & 6d), since its large ellipse arc edge curvature possess much stronger arc edge pinning effects at the spanwise of the arc edge, *i.e.* the intersection of CA and RE. Such a sharp arc edge can effectively keep the liquid pinned even when dropping complete wetting liquid on the surface (Fig. 1b). Uni-directional liquid spreading can finally be realized, as shown in E190, $\beta = 50°$ (Fig. 3b and 4b).

3. Conclusions

In summary, inspired by the arc-shaped sharp edge and wedge corner of duck-billed microcavities in *N. alata*, a novel uni-

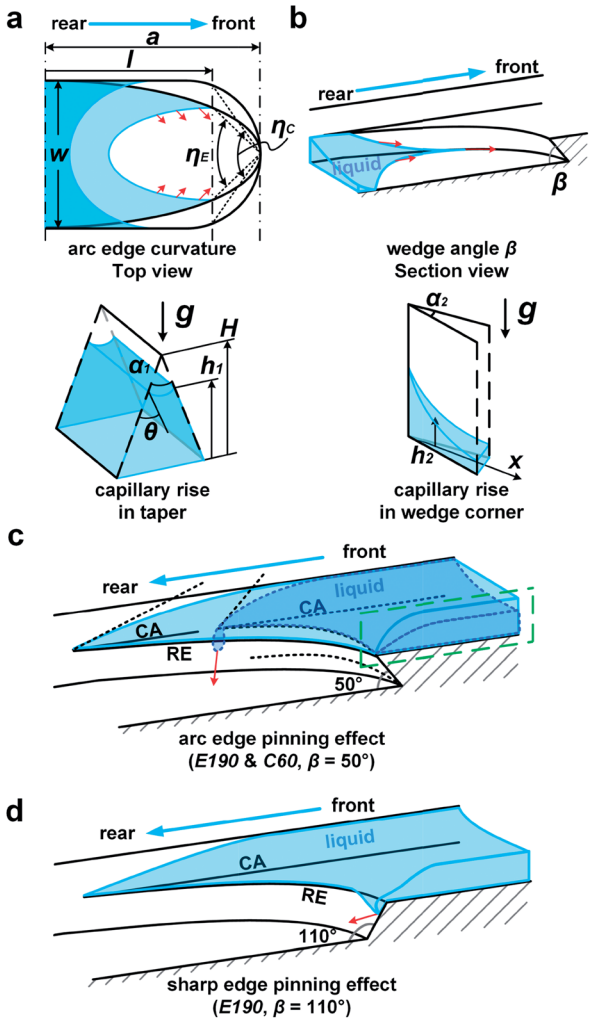

Fig. 6 Mechanisms of liquid uni-directional spreading. (a) Liquid spreading in microgrooves with different arc edge curvatures (top) can be regarded as liquid capillary rise in a taper with various cone angles α_1 (bottom). w is the width of the channel. a and l are the semi-major axis length and the distance from the center of the ellipse arc to the liquid contact line. η_C and η_E are the open angle of the circle arc and ellipse arc at the position of l. g, θ and H are the gravitational acceleration, the contact angle of the liquid and the height of the horizontal wedge corner. h_1 represents the height of liquid capillary rising. (b) The influence of the microcavity wedge angle β on liquid spreading (top) can be regarded as capillary rise in a wedge corner with different open angles of α_2 (bottom). h_2 denotes the height of liquid capillary rising in a vertical wedge corner at the position of x. (c) Arc edge pinning effect induced by different arc edge curvatures (E190 and C60, $\beta = 50°$). Liquid in C60 breaks through the pinning barrier at the intersection of RE and CA. RE and CA represent the rear edge and corner A, respectively. (d) In a sharp edge pinning failure, liquid breaks the pinning through the center of RE (E190, $\beta = 110°$).

directional liquid spreading surface structure has been designed and fabricated *via* the use of two-step inclined UV exposure photolithography. Complete wetting was proved to be essential for perfect uni-directional liquid spreading through investigating the effects of surface wettability on anisotropic liquid spreading. Moreover, two main structural features, *i.e.* arc edge curvature and microcavity wedge angle β, which were extracted from the peristome, were another two important factors for uni-directional liquid spreading. Particularly, a large arc edge curvature and small wedge angle β can assist much stronger uni-directional liquid spreading ability. The underlying uni-directional liquid spreading mechanism was also provided for each surface feature, and anisotropic liquid spreading can be controlled using these features. These bio-inspired uni-directional liquid spreading surface structures can advance a variety of applications such as non-power driven biochemical devices,[30] microfluidic electrochemical devices[31] and even self-lubrication in mechanical engineering.

4. Experimental section

4.1 Bio-inspired surface fabrication

The bio-inspired surfaces were fabricated *via* two-step UV photolithography. An inclined pitted array was built with inclined UV exposure on a 30 μm thick SU-8 photoresist as the first step. In the second step, microgrooves were constructed to just cover one line of inclined pits. Various types of masking pattern and UV inclined angles were prepared in the first step for surface fabrication with different arc edge curvatures and wedge angles.

4.2 Characterization of uni-directional liquid spreading with different surface wettability

Various wettable surfaces were obtained *via* different plasma treatment durations, including 5, 3, 1 and 0.5 min with a contact angle of about 5°, 37°, 47° and 64°, respectively. A volume of 0.1 μL of liquid was injected into the center of the microgrooves.

4.3 *In situ* observation of liquid spreading on different surface structures

About 0.1 μL of ethanol was used and injected into the center of microgrooves in 0.1 s using a micro injector (RSP01-BG, RISTRON Inc.). *In situ* observation of liquid spreading was conducted using a high-speed camera (I-speed LT, Olympus, Japan) with a recording speed of 800 frames per second. The time was recorded with the liquid spreading past each structural period.

Acknowledgements

This work was supported by the NSFC Major Program (No. 51290292).

Notes and references

1 A. R. Parker and C. R. Lawrence, *Nature*, 2001, **414**, 33–34.
2 Y. M. Zheng, H. Bai, Z. B. Huang, X. L. Tian, F. Q. Nie, Y. Zhao, J. Zhai and L. Jiang, *Nature*, 2010, **463**, 640–643.
3 J. Ju, H. Bai, Y. M. Zheng, T. Y. Zhao, R. C. Fang and L. Jiang, *Nat. Commun.*, 2012, **3**, 1247.
4 I. E. Agranovski and R. D. Braddock, *AIChE J.*, 1998, **44**, 2775–2783.
5 M. A. Burns, C. H. Mastrangelo, T. S. Sammarco, F. P. Man, J. R. Webster, B. N. Johnsons, B. Foerster, D. Jones, Y. Fields

and A. R. Kaiser, *Proc. Natl. Acad. Sci. U. S. A.*, 1996, **93**, 5556–5561.
6 M. Grunze, *Science*, 1999, **283**, 41.
7 H. Gau, S. Herminghaus, P. Lenz and R. Lipowsky, *Science*, 1999, **283**, 46–49.
8 S. Daniel, M. K. Chaudhury and J. C. Chen, *Science*, 2001, **291**, 633–636.
9 H. W. Chen, L. W. Zhang, D. Y. Zhang, P. F. Zhang and Z. W. Han, *ACS Appl. Mater. Interfaces*, 2015, **7**, 13987–13995.
10 F. Brochard, *Langmuir*, 1989, **5**, 432–438.
11 M. K. Chaudhury and G. M. Whitesides, *Science*, 1992, **256**, 1539–1541.
12 J. B. Brzoska, F. Brochard-Wyart and F. Rondelez, *Langmuir*, 1993, **9**, 2220–2224.
13 A. L. Yarin, W. Liu and D. H. Reneker, *J. Appl. Phys.*, 2002, **91**, 4751–4760.
14 L. Wang, C. L. Gao, Y. P. Hou, Y. M. Zheng and L. Jiang, *J. Mater. Chem. A*, 2016, **4**, 18289–18293.
15 H. Bai, X. L. Tian, Y. M. Zheng, J. Ju, Y. Zhao and L. Jiang, *Adv. Mater.*, 2010, **22**, 5521–5525.
16 X. Y. Ma, M. Y. Cao, C. Teng, H. Li, J. S. Xiao, K. S. Liu and L. Jiang, *J. Mater. Chem. A*, 2015, **3**, 15540–15545.
17 J. Li, Q. H. Qin, A. Shah, R. H. Ras, X. Tian and V. Jokinen, *Sci. Adv.*, 2016, **2**, e1600148.
18 K. H. Chu, R. Xiao and E. N. Wang, *Nat. Mater.*, 2010, **9**, 413–417.
19 J. X. Wang, Y. Q. Wen, J. P. Hu, Y. L. Song and L. Jiang, *Adv. Funct. Mater.*, 2007, **17**, 219–225.
20 F. Xia, L. Feng, S. T. Wang, T. L. Sun, W. L. Song, W. H. Jiang and L. Jiang, *Adv. Mater.*, 2006, **18**, 432–436.
21 W. Q. Zhu, X. J. Feng, L. Feng and L. Jiang, *Chem. Commun.*, 2006, 2753–2755.
22 P. F. Zhang, H. W. Chen, L. Li, H. L. Liu, G. Liu, L. W. Zhang, D. Y. Zhang and L. Jiang, *ACS Appl. Mater. Interfaces*, 2017, **9**, 5645–5652.
23 H. Bai, J. Ju, R. Sun, Y. Chen, Y. Zheng and L. Jiang, *Adv. Mater.*, 2011, **23**, 3708–3711.
24 E. Lorenceau and D. Quere, *J. Fluid Mech.*, 2004, **510**, 29–45.
25 J. L. Zhang and Y. C. Han, *Langmuir*, 2007, **23**, 6136–6141.
26 H. W. Chen, P. F. Zhang, L. W. Zhang, H. L. Liu, Y. Jiang, D. Y. Zhang, Z. W. Han and L. Jiang, *Nature*, 2016, **532**, 85–89.
27 H. W. Chen, L. W. Zhang, P. F. Zhang, D. Y. Zhang, Z. W. Han and L. Jiang, *Small*, 2017, **13**, 1601676.
28 Z. J. Wang, C. C. Chang, S. J. Hong, Y. J. Sheng and H. K. Tsao, *Langmuir*, 2012, **28**, 16917–16926.
29 J. F. Oliver, C. Huh and S. G. Mason, *J. Colloid Interface Sci.*, 1977, **59**, 568–581.
30 J. F. Tian, D. Kannangara, X. Li and W. Shen, *Lab Chip*, 2010, **10**, 2258–2264.
31 F. F. Shao, T. W. Ng, J. Fu, W. Shen and W. Y. L. Ling, *J. Colloid Interface Sci.*, 2011, **363**, 425–430.